Supporting Information

Wontakal et al. 10.1073/pnas.1121019109

SI Materials and Methods

ChIP-Seq Data Analysis. All reads (36 bp) from the GATA-1 ChIP-Seq were mapped to the mouse genome (version mm9 or build 37) by the ELAND aligner within the Illumina Analysis Pipeline. Aligned reads with a single best matching location and up to two mismatches were retained for peak identification. As genome-wide binding profiles from replicate chromatin immunoprecipitation and high-throughput sequencing (ChIP-Seq) runs were highly correlated (data not shown), we combined aligned reads from replicates and obtained a total of 9,486,136 and 18,717,198 uniquely mapped reads from embryonic stem cell-derived erythroid progenitor (ES-EP) proliferating and differentiating cells, respectively. For input DNA controls, 7,488,885 and 8,535,843 reads were obtained for each of these two respective conditions. The program spp (1) was applied to call peaks, genomic regions of significant GATA-1 occupancy, by comparing reads from the immunoprecipitated (IP) sample to the corresponding input DNA sample. To estimate parameters for final peak calling, we initially called peaks for replicated data independently and then the combined data and calculated the overlaps of peaks from the combined reads with the union of peaks from two individual replicates. Afterward, we selected spp parameters to maximize the overlaps that also yield comparable peak numbers between proliferating and differentiating conditions. The final spp parameters were scored >8 and enrichment.lb >1, with the rest set to defaults, which resulted in 6,600 and 10,600 GATA-1 peaks in proliferating and differentiating ES-EP cells, respectively.

For each GATA-1 peak we extracted a 500-bp sequence around the peak center (i.e., ±250 bp) and used it for de novo motif discovery by the MEME software (2). The known consensus GATA-1 binding motif was the top motif returned by MEME for both proliferating and differentiating conditions, and 95% andi 79% of peaks were found to contain the consensus motif, respectively.

To associate peaks with target genes, we tested several criteria, assigning genes with GATA-1 peaks from −2 kb, −10 kb, or −20 kb of transcription start sites (TSS) to +10 kb of transcription end sites (TES). In addition, we also tested assigning peaks to the closest gene. As a group, GATA-1 targets resulting from the first three criteria did not show significant differences of GATA-1–dependent gene expression except when they were compared with the last group on the basis of the nearest distance (Fig. S3). Accordingly, we chose −20 kb of TSS to +10 kb of TES as the criterion for assigning a peak to a gene. The same criterion was used to assign ChIP-Seq peaks for PU.1, Klf1, and SCL to genes. Totals of 1,380 Klf1 peaks and 2,994 SCL peaks were collected from previous studies by Tallack et al. (3) and Kassouf et al. (4) performed with fetal-liver erythroid progenitors, and PU.1 peaks (16,241) were obtained from our previous ChIP-Seq analysis in ES-EP cells (5). Gene targets were separated into groups on the basis of the co-occupancy pattern of these four transcription factors, and these groups were subjected to functional analysis with Ingenuity Pathway Analysis and DAVID GO analysis (6).

Gene Expression Analysis. Acquisition of gene expression data for proliferating and differentiating ES-EP and murine erythroleukemia (MEL) cells and fetal-liver erythroid progenitors from wild-type and PU.1 URE$^{-/-}$ was described previously (5) and can be accessed from the National Center for Biotechnology Information's Gene Expression Omnibus (GEO) database using accession no. GSE21953. Microarray data were normalized by the RMA method in the GeneSpring GX software. The $\log_2$ transformed signal intensities were averaged for biological replicates and used for computing expression fold change. Heat maps were generated with the mean value of all time points for a given gene and assigned a color gradient for each time point by calculating the $\log_2$ ratio of that time point to the mean expression value. GATA-1–dependent gene expression data were downloaded from the GEO database using accession no. GSE18042 (7). After data normalization, the fold change in expression of a gene was calculated by comparing its expression value at 0 h with the average value of all other time points. Klf1- and SCL-dependent expression data were obtained from Hodge et al. (8) and the GEO database using accession no. GSE21877 (4), respectively. The signal intensities were $\log_2$ transformed and quartile normalized. Fold changes in gene expression were determined with the limma algorithm (9) in the Bioconductor package.

e4c Interaction Data. A total of 551 and 273 e4C genomic clusters interacting with Hba and Hbb, respectively, and a total of 6,396 highly transcribed genes (by RNAPII-S5P occupancy) were obtained from Schoenfelder et al. (10). Active Hba- and Hbb-interacting genes in erythroid cells were defined as transcribed genes within the e4C clusters, as described previously (10). Overrepresentation of active e4C genes in different groups was calculated using the hypergeometric probability distribution.

Statistical Analysis. Wilcoxon signed rank tests were applied to compare differences in gene expression changes between any two groups of genes with designated patterns of transcriptional factor occupancy. A binomial test was applied to calculate the enrichment of genes occupied by three factors, respectively, in all genes from the mouse genome, erythroid-specific genes, and genes highly expressed in the erythroid lineage. All statistical analyses were carried out in the R language.

Mathematical Modeling. A system of four coupled nonlinear ordinary differential equations is used to model the GATA-1–PU.1 regulatory network:

$$\frac{dG}{dt} = \underbrace{G_s}_{1} + \underbrace{k_{ar}\frac{G^n}{K_{ar}^n + G^n}\frac{K_{ir}^n}{K_{ir}^n + P^n}}_{2} - \underbrace{k_d G}_{3}, \qquad [S1]$$

$$\frac{dP}{dt} = P_s + k_{ar}\frac{P^n}{K_{ar}^n + P^n}\frac{K_{ir}^n}{K_{ir}^n + G^n} - k_d P, \qquad [S2]$$

$$\frac{dG_T}{dt} = \underbrace{k_{at}\frac{G}{K_{at} + G}}_{1} + \underbrace{k_{at}\frac{K_{it}}{K_{it} + P}}_{2} - \underbrace{k_d G_T}_{3}, \qquad [S3]$$

$$\frac{dP_T}{dt} = k_{at}\frac{P}{K_{at} + P} + k_{at}\frac{K_{it}}{K_{it} + G} - k_d P_T. \qquad [S4]$$

The state variables of the preceding system of equations can be interpreted according to the following definitions: G, GATA-1 concentration; P, PU.1 concentration; G_T, GATA-1 target concentration; and P_T, PU.1 target concentration. The parameter values are labeled with subindexes a, activation; i, inhibition; d, degradation; r, regulator; t, target; s, stimulus. G_s and P_s are the

GATA-1 and PU.1 stimulation rates; n is the Hill coefficient; k_{ar} and k_{at} are maximal activation rates; K_{ar}, K_{at}, K_{ir}, and K_{it} are half-maximal concentrations for activation or inhibition as indicated by subscripts; and k_d is the first-order degradation rate assumed to be equal for all species included in the model.

To demonstrate the independence of the model from a particular choice of units for time and concentration, it is possible to introduce a change of variables that enables the expression of all parameter values as dimensionless quantities according to the Buckingham π-theorem (11). For example, time can be scaled by the degradation rate (which has units time^{-1}) rather than specifying an arbitrary scale. This process demonstrates the capacity to eliminate redundant dimensions from the parameter space of the model. We therefore derive a dimensionless form for the model of Eqs. **S1**–**S4** in Eqs. **S5**–**S8**:

$$\frac{d\gamma}{d\tau} = \gamma_s + \kappa_r \frac{\gamma^n}{1+\gamma^n}\frac{\lambda_r^n}{\lambda_r^n+\pi^n} - \gamma, \qquad \textbf{[S5]}$$

$$\frac{d\pi}{d\tau} = \pi_s + \kappa_r \frac{\pi^n}{1+\pi^n}\frac{\lambda_r^n}{\lambda_r^n+\gamma^n} - \pi, \qquad \textbf{[S6]}$$

$$\frac{d\gamma_T}{d\tau} = \kappa_t\left(\frac{\gamma}{\alpha+\gamma} + \frac{\lambda_t}{\lambda_t+\pi}\right) - \gamma_T, \qquad \textbf{[S7]}$$

$$\frac{d\pi_T}{d\tau} = \kappa_t\left(\frac{\pi}{\alpha+\pi} + \frac{\lambda_t}{\lambda_t+\gamma}\right) - \pi_T. \qquad \textbf{[S8]}$$

In the derivation of the dimensionless Eqs. **S5**–**S8** the state variables and time from Eqs. **S1**–**S4** have been scaled according to the following relationships: $\gamma = \frac{G}{K_{ar}}$, $\pi = \frac{P}{K_{ar}}$, $\gamma_T = \frac{G_T}{K_{at}}$, $\pi_T = \frac{P_T}{K_{at}}$, and $\tau = k_d t$. The relationship between the parameter values of the dimensional and dimensionless forms of the model along with an associated set of base parameter values is presented in Table S1. Selecting values for the dimensionless parameters induces the definition of an equivalence class of dimensional models that all exhibit similar qualitative behavior where the relationships among the dimensioned parameter values result in the corresponding values for the dimensionless parameters. Our numerical simulations of Eqs. **S1**–**S4** are based upon a member of the equivalence class defined by the parameter values in Table S1. Note that the parameter values K_{ir} and K_{it} (equivalently λ_r and λ_t) are modulated in numerical simulations to compare alternative network topologies (Table S2).

Here we define the assumptions of the model with reference to variables and parameter values in Eqs. **S1**–**S4**. Identical assumptions apply to Eqs. **S5**–**S8**. To model the GATA-1/PU.1 regulatory network we assume that the network architecture for GATA-1 and its targets is symmetric to that for PU.1 and its targets. Somewhat more formally, there is a permutation symmetry among the state variables representing GATA-1 and PU.1 as well as GATA-1 targets and PU.1 targets as demonstrated by the invariance of the model under the set of transformations $\sigma : \{G \leftrightarrow P, G_T \leftrightarrow P_T, G_s \leftrightarrow P_s\}$. We introduce asymmetry only in the upstream stimuli (e.g., erythropoietin and GM-CSF represented by the relative magnitudes and duration of G_s and P_s). In Eqs. **S1** and **S2**, G_s and P_s, respectively represent GATA-1 and PU.1 upstream stimulation rates. The second terms of Eqs. **S1** and **S2** consist of three components. The first is the maximal activation rate described by the parameter k_{ar}. The second parts are Hill functions describing the autoregulation of GATA-1 and PU.1 with half-maximal activation constants K_{ar} (12). The corresponding Hill coefficients, n, in the base parameter set are >1 to represent the existence of multiple binding sites for GATA-1 and PU.1 in the upstream regulatory regions of the GATA-1 and PU.1 genes (13–15). The third parts are Hill functions representing the mutual inhibition of PU.1 and GATA-1 on each other's gene expression with half-maximal inhibition constants K_{ir}. Qualitatively identical results are obtained even if the Hill coefficients in the autoregulatory and cross-inhibition terms are independent for all combinations of Hill coefficients in the range we tested: $n = 2, \ldots, 6$. The autoregulatory and cross-inhibition components of the second terms are multiplied by one another to represent their competition to control the synthesis rates of GATA-1 and PU.1. The final terms of Eqs. **S1** and **S2** represent first-order degradation processes with rates k_d for both GATA-1 and PU.1. Eqs. **S3** and **S4** represent the dynamics of GATA-1 and PU.1 targets, respectively. The first term of Eq. **S3** represents GATA-1–mediated activation of its targets with half-maximal activation constant K_{at}, the second term is PU.1 inhibition of the expression of GATA-1 targets with half-maximal inhibition constant K_{it}, and the third term is the first-order degradation with rate k_d of the GATA-1 targets. We have assumed that GATA-1 and PU.1 serve as independent inputs to their respective target genes. The terms of Eq. **S4** are analogous to those of Eq. **S3** but describe the regulation of PU.1 targets. The overall form of Eqs. **S1**–**S4** is similar to that proposed by Laslo et al. to model a different aspect of the hematopoietic gene regulatory network (16). This system of equations is symmetric for GATA-1 and PU.1 and therefore the differential stimulus applied to favor GATA-1 and the erythroid cell fate over PU.1 and the myeloid cell fate in the test case shown in Fig. 4 would produce precisely the opposite result (i.e., PU.1-mediated myeloid lineage differentiation as opposed to GATA-1–mediated erythroid lineage differentiation were the stimuli magnitudes permuted).

Characterization of the Mathematical Model. To understand the function of the GATA-1–PU.1 network topology identified experimentally (Fig. S7*D*) we investigated the effects of continuous modulation of the network topology upon the cell fate determination specified by the ratio between the steady-state expression levels of GATA-1 and PU.1 target genes. The model was evaluated via numerical simulations in which GATA-1 receives an initial transient stimulus G_S that is 10-fold higher than that applied to PU.1 (Figs. S8–S11 and Table S1). To produce the network topology shown in Fig. S7*A* given the system of Eqs. **S1**–**S4** we require the parameters K_{ir} and K_{it} to take values that are high relative to the maximal protein concentrations. To modulate the network topology from that of Fig. S7*A* (bottom center corner of Fig. 4*A*) to that of Fig. S7*B* (right corner of Fig. 4*A*) we varied the parameter K_{ir} along this axis (the x axis) from high [Max(K) = 10^3] to low [Min(K) = 10^{-1}]. However, for clarity of presentation, on the x axis of Fig. 4 we transformed the K_{ir} values using the following function $f(K)$ = Max(K) − Min(K) − K_j, where K represents the vector of K_{ir} values $K = \{K_j\}$, thus representing the antagonistic interaction *strength*. We transformed the K_{it} values in the same way to represent antagonistic interaction strengths along the y axes of Fig. 4. When K_{ir} is high, the terms $\frac{K_{ir}^n}{K_{ir}^n+P^n}$ and $\frac{K_{ir}^n}{K_{ir}^n+G^n}$ from Eqs. **S1** and **S2**, respectively, are ≈ 1 and therefore neither GATA-1 nor PU.1 inhibits the expression of the other. As K_{ir} decreases, the concentrations of GATA-1 and PU.1 play increasingly significant roles as inhibitors of the expression of the other and, in the case when either GATA-1 or PU.1 reaches extremely high levels, these terms approach zero. The network topology is similarly modulated from that of Fig. S7*A* to that of Fig. S7*C* by decreasing the value of the parameter K_{it}. The network topology represented in Fig. S7*D* is produced when both K_{ir} and K_{it} take on low values relative to the maximal protein concentrations.

To characterize the dynamics of GATA-1–PU.1 regulation near each of the four corners of the K_{ir} – K_{it} parameter space represented in the xy plane of Fig. 4*A* we simulated Eqs. **S1**–**S4** for four

different combinations of $K_{ir} - K_{it}$ parameter values described with their corresponding network topologies in Table S2.

The dynamics for each parameter set listed in Table S2 are displayed in Figs. S8–S11. Note that when the mutual inhibition is low regardless of the state of inhibition of the downstream targets, the G_T/P_T ratio is low given the 10:1 G_s/P_s asymmetric input (Figs. S8 and S10). When the mutual inhibition is increased, the G_T/P_T ratio increases, even with relatively low inhibition of the downstream targets (Fig. S9); however, when inhibition of the downstream targets is increased following an increase in the mutual inhibition, the most significant increase in the G_T/P_T ratio occurs (Fig. S11). This result is consistent with the theoretically and experimentally corroborated conclusion stated in the main text that mutual inhibition and repression of downstream targets act synergistically to produce a high-fidelity mapping from upstream cell-fate determining signals to the cell fate specified by a particular downstream gene expression program.

1. Kharchenko PV, Tolstorukov MY, Park PJ (2008) Design and analysis of ChIP-seq experiments for DNA-binding proteins. *Nat Biotechnol* 26:1351–1359.
2. Bailey TL, Elkan C (1994) Fitting a mixture model by expectation maximization to discover motifs in biopolymers. *Proc Int Conf Intell Syst Mol Biol* 2:28–36.
3. Tallack MR, et al. (2010) A global role for KLF1 in erythropoiesis revealed by ChIP-seq in primary erythroid cells. *Genome Res* 20:1052–1063.
4. Kassouf MT, et al. (2010) Genome-wide identification of TAL1's functional targets: Insights into its mechanisms of action in primary erythroid cells. *Genome Res* 20:1064–1083.
5. Wontakal SN, et al. (2011) A large gene network in immature erythroid cells is controlled by the myeloid and B cell transcriptional regulator PU.1. *PLoS Genet* 7:e1001392.
6. Dennis G, Jr., et al. (2003) DAVID: Database for Annotation, Visualization, and Integrated Discovery. *Genome Biol* 4:3.
7. Cheng Y, et al. (2009) Erythroid GATA1 function revealed by genome-wide analysis of transcription factor occupancy, histone modifications, and mRNA expression. *Genome Res* 19:2172–2184.
8. Hodge D, et al. (2006) A global role for EKLF in definitive and primitive erythropoiesis. *Blood* 107:3359–3370.
9. Smyth GK (2004) Linear models and empirical Bayes methods for assessing differential expression in microarray experiments. *Stat Appl Genet Mol Biol* 3:Article3.
10. Schoenfelder S, et al. (2010) Preferential associations between co-regulated genes reveal a transcriptional interactome in erythroid cells. *Nat Genet* 42:53–61.
11. Gibbings JC (2011) *Dimensional Analysis* (Springer, Heidelberg), 1st Ed, pp 55–82.
12. Huang S, Guo YP, May G, Enver T (2007) Bifurcation dynamics in lineage-commitment in bipotent progenitor cells. *Dev Biol* 305:695–713.
13. Kobayashi M, Yamamoto M (2007) Regulation of GATA1 gene expression. *J Biochem* 142:1–10.
14. Zarnegar MA, Chen J, Rothenberg EV (2010) Cell-type-specific activation and repression of PU.1 by a complex of discrete, functionally specialized cis-regulatory elements. *Mol Cell Biol* 30:4922–4939.
15. Leddin M, et al. (2011) Two distinct auto-regulatory loops operate at the PU.1 locus in B cells and myeloid cells. *Blood* 117:2827–2838.
16. Laslo P, et al. (2006) Multilineage transcriptional priming and determination of alternate hematopoietic cell fates. *Cell* 126:755–766.

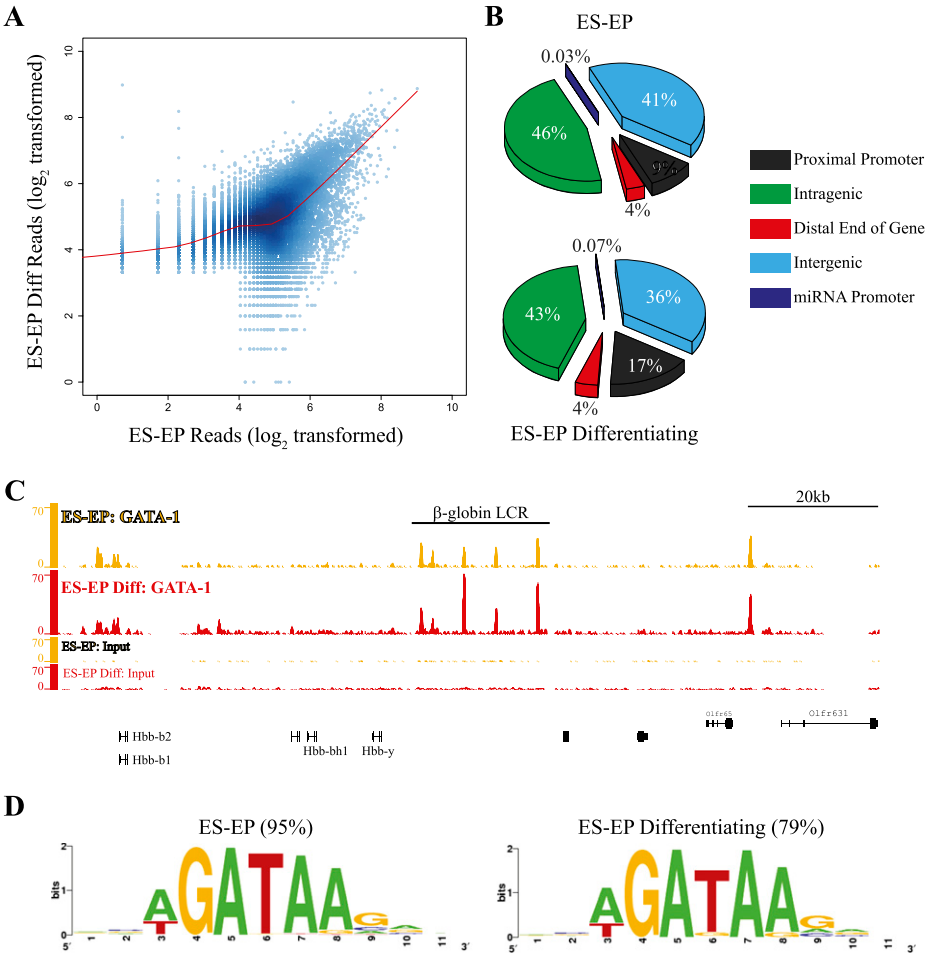

Fig. S1. Properties of GATA-1 ChIP-Seq peaks. (*A*) Comparison of GATA-1 ChIP-Seq peaks in proliferating and differentiating ES-EP. The number of reads ($\log_2$ transformed) in each GATA-1 ChIP-Seq peak present in the two types of cells is shown for proliferating ES-EP (abscissa) and differentiating ES-EP (ordinate). The red line represents local quantile and Lowess regression fitting. The correlation coefficient for the data displayed is 0.68 ($P < 2.2e\text{-}16$). (*B*) GATA-1 ChIP-Seq peaks were annotated by their genomic locations with respect to current gene annotation and classified as proximal promoter (±2 kb of TSS), 3′ end of gene (±2 kb of TES), gene body (between +2 kb of TSS and −2 kb of TES), miRNA promoters, or otherwise intergenic regions. (*C*) Sample signal tracks of GATA-1 ChIP-Seq data from ES-EP and differentiating ES-EP (ES-EP Diff) ∼100-kb region near the β-globin locus in the Integrated Genome Browser (IGB) (Affymetrix) with the *y* axis representing the number of reads. Input DNA controls for both cell types are also shown. (*D*) Sequence logos for the enriched motifs within GATA-1 ChIP-Seq peaks from ES-EP (*Left*) and differentiating ES-EP (*Right*) were derived from MEME motif analysis (*SI Materials and Methods*). The percentage of peaks with the motif is also shown.

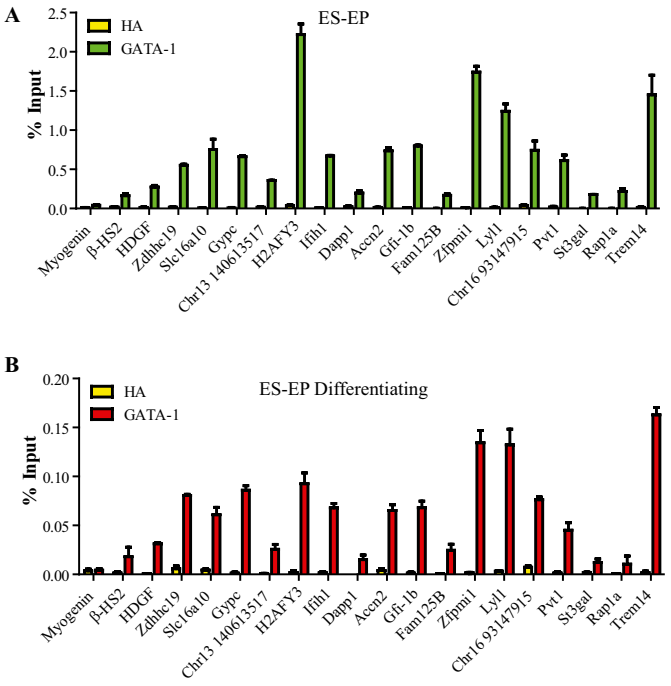

Fig. S2. qChIP validation of GATA-1 occupancy. qChIP was performed as described in *SI Materials and Methods* with chromatin from proliferating (*A*) and differentiating (*B*) ES-EP with primers described in Table S3. Myogenin and β-HS2 served as negative and positive control loci, respectively. HA antibody was used as an isotype control. SDs were calculated from triplicate PCR reactions. Similar results were obtained with at least two independent chromatin preparations.

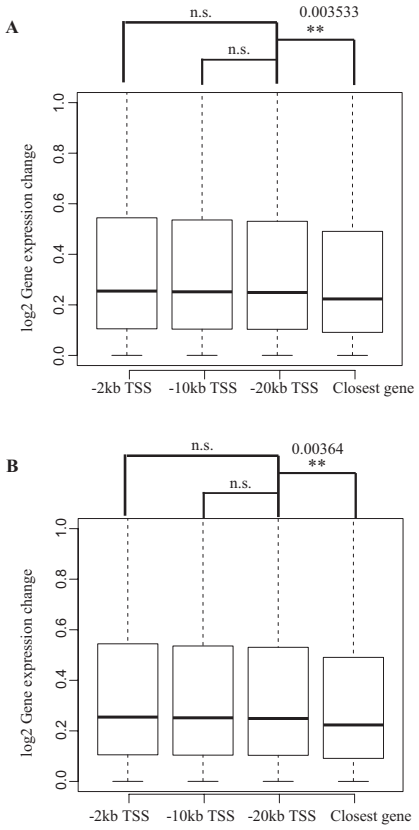

Fig. S3. Analysis of four different criteria for assigning GATA-1 ChIP-Seq peaks to genes. GATA-1 ChIP-Seq peaks in proliferating ES-EP (*A*) and differentiating ES-EP (*B*) were assigned to genes on the basis of four different criteria: (*i–iii*) assignment if the peak lies within the region spanning from −2 kb (*i*), −10 kb (*ii*), and −20 kb (*iii*) of a TSS through +10 kb of the TES and (*iv*) assignment of the peak to the nearest gene. Using these four assignment criteria and published GATA-1–dependent gene expression changes in erythroid cells (1, 2), boxplots were constructed to show the $\log_2$ fold change in expression of the four different sets of genes.

1. Cheng Y, et al. (2009) Erythroid GATA1 function revealed by genome-wide analysis of transcription factor occupancy, histone modifications, and mRNA expression. *Genome Res* 19: 2172–2184.
2. Yu M, et al. (2009) Insights into GATA-1-mediated gene activation versus repression via genome-wide chromatin occupancy analysis. *Mol Cell* 36:682–695.

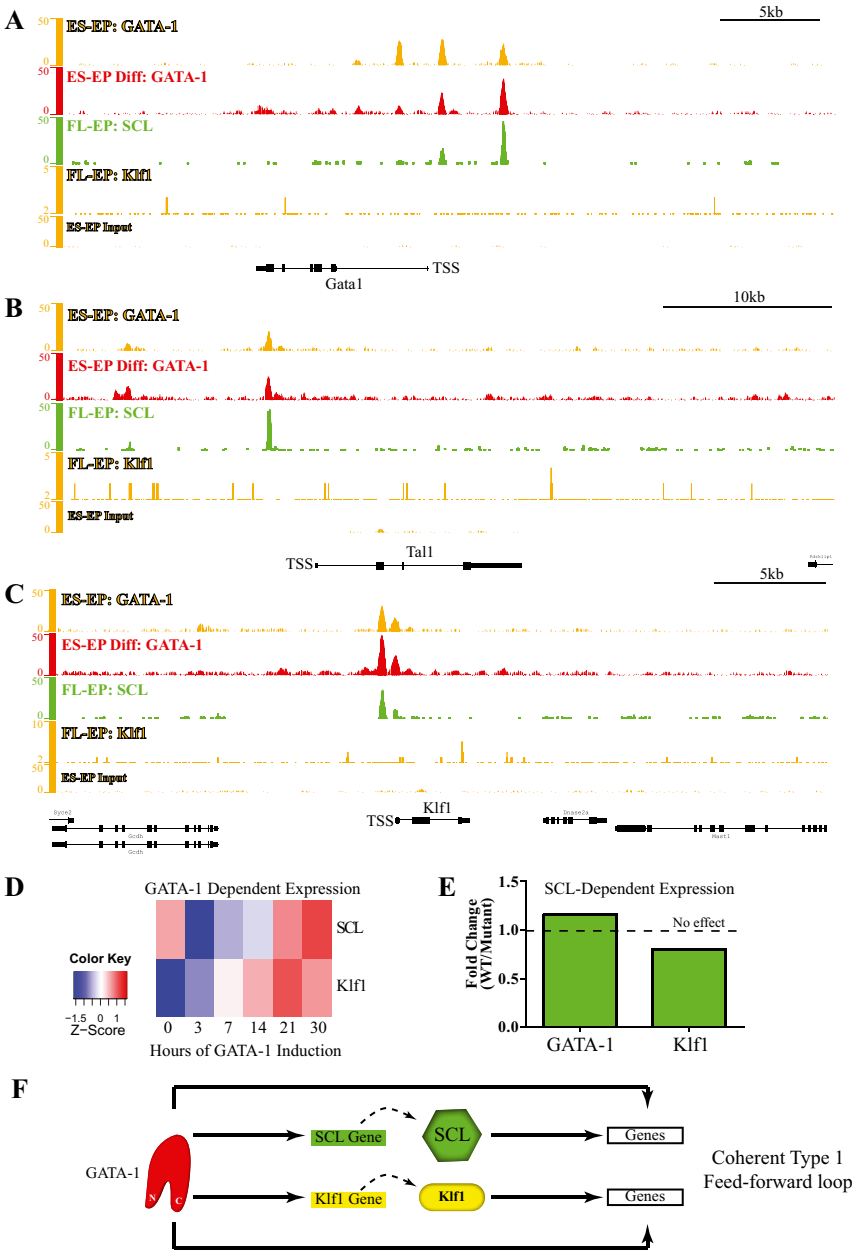

Fig. S4. GATA-1 acts upstream of SCL and Klf1. (*A–C*) Occupancy maps from ChIP-Seq data for GATA-1 in proliferating and differentiating ES-EP and for SCL and Klf1 in FL-EP are shown in the vicinity of the genes encoding GATA-1 (*A*), SCL (Tal1) (*B*), and Klf1 (*C*). (*D*) Heatmap of GATA-1–dependent changes in gene expression (1, 2) of SCL and Klf1. (*E*) Gene expression differences for GATA-1 and Klf1 between FL-EP from wild-type and SCL DNA-binding–defective mutant mice (3). (*F*) A model for a coherent type 1 feed-forward loop formed by GATA-1 and SCL and by GATA-1 and Klf1 based on the ChIP-Seq and gene expression data displayed in *A–E*.

1. Cheng Y, et al. (2009) Erythroid GATA1 function revealed by genome-wide analysis of transcription factor occupancy, histone modifications, and mRNA expression. *Genome Res* 19: 2172–2184.
2. Yu M, et al. (2009) Insights into GATA-1-mediated gene activation versus repression via genome-wide chromatin occupancy analysis. *Mol Cell* 36:682–695.
3. Kassouf MT, et al. (2010) Genome-wide identification of TAL1's functional targets: Insights into its mechanisms of action in primary erythroid cells. *Genome Res* 20:1064–1083.

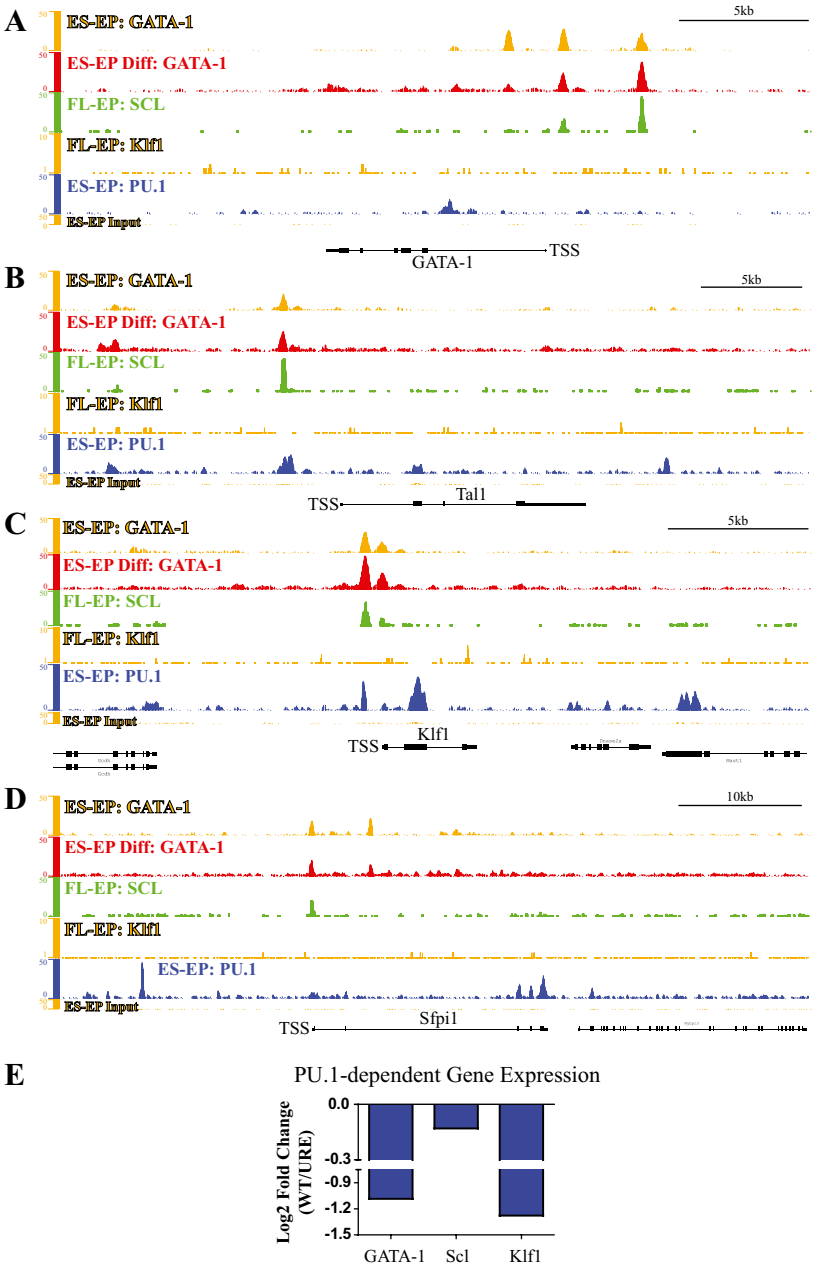

Fig. S5. PU.1 binds near to the GATA-1, SCL, and Klf1 genes and represses their expression. (*A*–*D*) Occupancy maps from ChIP-Seq data for GATA-1, SCL, Klf1, and PU.1 in the vicinity of the genes encoding (*A*) GATA-1, (*B*) SCL (Tal1), (*C*) Klf1, and (*D*) PU.1 (Sfpi1). (*E*) Log_2 fold change in gene expression of GATA-1, SCL, and Klf1 in PU.1-depleted ($URE^{-/-}$) vs. wild-type early FL-EP (5).

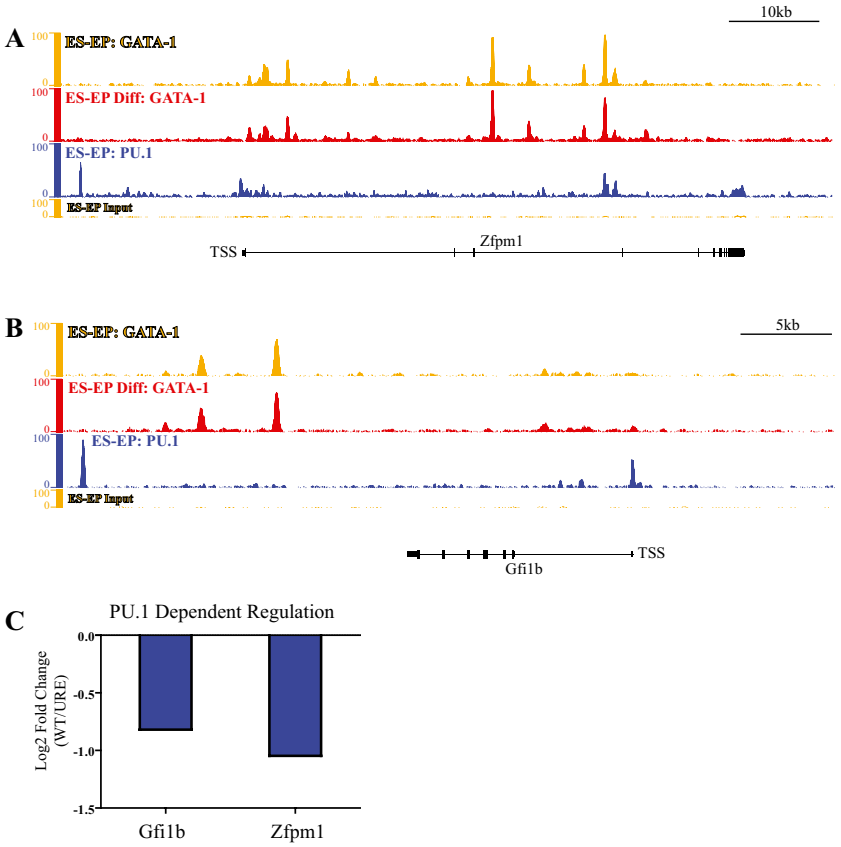

Fig. S6. PU.1 binds near the genes encoding two important cofactors of GATA-1 and represses their expression. (*A* and *B*) Occupancy maps from ChIP-Seq data for GATA-1 and PU.1 near the genes encoding (*A*) FOG1 (Zfpm1) and (*B*) Gfi1b. (*C*) Log_2 fold change in gene expression of Zfpm1 and Gfi1b in PU.1-depleted ($URE^{-/-}$) vs. wild-type early FL-EP. Data are from ref. 5.

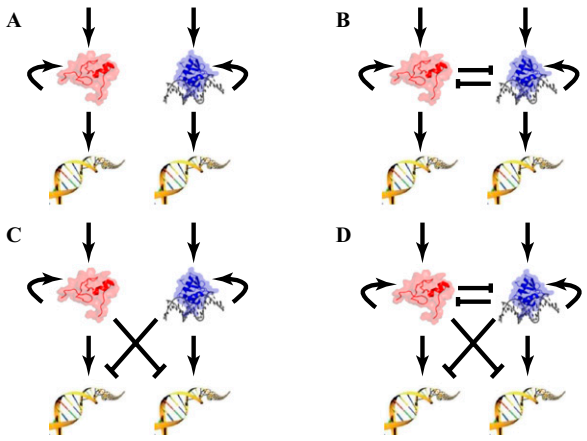

Fig. S7. (*A–D*) Description of four GATA-1–PU.1 regulatory network topologies. See Table S2 for examples of parameter value relationships that specify, in the mathematical model, each of the regulatory network topologies. Relevant limiting cases of the model are shown in parentheses following each description. (*A*) GATA-1 and PU.1, each regulated by an upstream stimulus, autoregulate themselves and activate mutually exclusive sets of downstream targets ($K_{ir} \to \infty$, $K_{it} \to \infty$). (*B*) Same as *A* but GATA-1 and PU.1 directly inhibit the expression of the other ($K_{ir} \to 0$, $K_{it} \to \infty$). (*C*) Same as *A* but GATA-1 and PU.1 inhibit the expression of the other's downstream targets ($K_{ir} \to \infty$, $K_{it} \to 0$). (*D*) Combination of *B* and *C* where GATA-1 and PU.1 both inhibit each other directly and inhibit the expression of the other's downstream targets ($K_{ir} \to 0$, $K_{it} \to 0$).

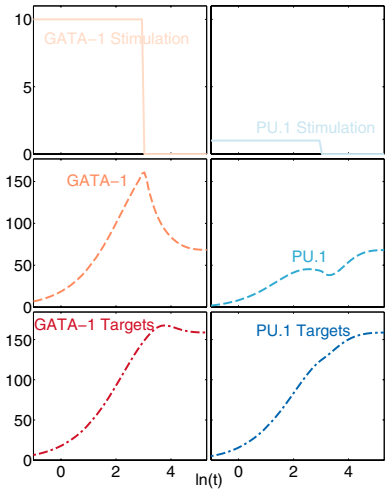

Fig. S8. Temporal dynamics for the network topology depicted in Fig. S7*A*. (*Top*) Upstream stimulus pulses for GATA-1 (G_s) (*Left*) and PU.1 (P_s) (*Right*). (*Middle*) Time-dependent changes in the concentrations of GATA-1 (*Left*) and PU.1 (*Right*). (*Bottom*) Time-dependent changes in the concentrations of GATA-1 (*Left*) and PU.1 (*Right*) -dependent transcripts. All *y*-axis units are arbitrary. Parameter values are all specified in Table S1 except for those that select the network topology K_{ir} = 100, K_{it} = 100.

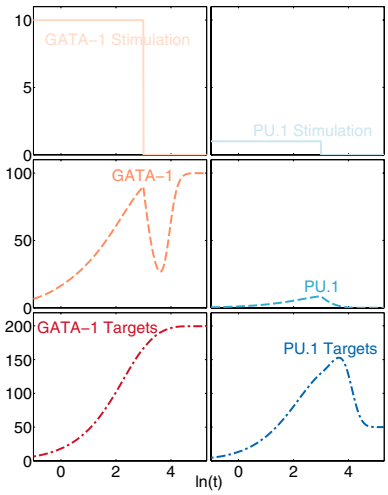

Fig. S9. Temporal dynamics for the network topology depicted in Fig. S7*B*. Layout and parameter values are the same as Fig. S8 except K_{ir} = 1, K_{it} = 100.

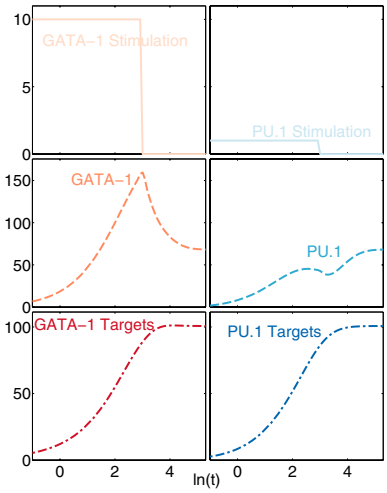

Fig. S10. Temporal dynamics for the network topology depicted in Fig. S7*C*. Layout and parameters are the same as Fig. S8 except K_{ir} = 100, K_{it} = 1.

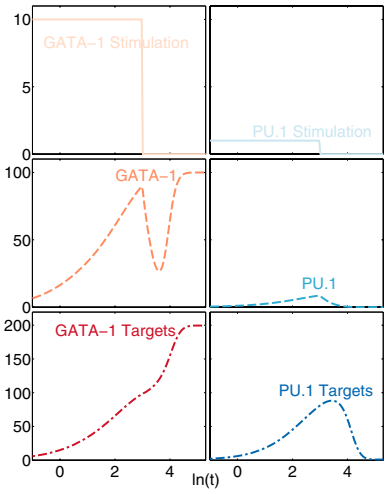

Fig. S11. Temporal dynamics for the network topology depicted in Fig. S7*D*. Layout and parameters are the same as Fig. S8 except K_{ir} = 1, K_{it} = 1.

Table S1. List of parameters with base values

Dimensionless parameters	Dimensioned parameters	Description	Base value(s)
κ_r	$\frac{k_{ar}}{k_d K_{ar}}$	Transcription factor maximal activation rate	10
λ_r	$\frac{K_{ir}}{K_{ar}}$	Transcription factor half-maximal inhibition constant	10^{-1}–10^{3}
κ_t	$\frac{k_{at}}{k_d K_{at}}$	Target maximal activation rate (per input)	10
λ_t	$\frac{K_{it}}{K_{ar}}$	Target half-maximal inhibition constant	10^{-1}–10^{3}
α	$\frac{K_{at}}{K_{ar}}$	Ratio of target to regulator half-maximal activation	1
γ_s	$\frac{G_s}{k_d K_{ar}}$	GATA-1 upstream stimulus	10× pulse
π_s	$\frac{P_s}{k_d K_{ar}}$	PU.1 upstream stimulus	1× pulse
n	n	Hill coefficient	2

Subscripts of parameter values can be interpreted according to these definitions: *a*, activation; *d*, degradation; *i*, inhibition; *r*, regulator; *s*, stimulus; *t*, target.

Table S2. Correspondence between network topologies and parameter values

Fig. 4*A* corner	Fig. S7	Figure containing dynamics	K_{ir}	K_{it}	Direct cross-inhibition strength	Downstream target inhibition strength
Center bottom	*A*	Fig. S8	100	100	Low	Low
Right	*B*	Fig. S9	1	100	High	Low
Left	*C*	Fig. S10	100	1	Low	High
Center top	*D*	Fig. S11	1	1	High	High

Table S3. List of qChIP primers

Gene	Forward primer	Reverse primer	Reference
Myogenin	GAA TCA CAT GTA ATC CAC TGG A	ACG CCA ACT GCT GGG TGC CA	(1)
β-HS2	TGT GTT CAG CCT TGT GAG CCA GC	TGG ACT TCC TCC TAG AGA CCC AG	(2)
HDGF	CCA AGA AAG ATG TGG GAG GA	CTG CTG CAG AAA GCT GAT TG	This study
Zdhhc19	TTT GAG GGT GAG GGT CAA AG	CCA TTT CTG CCA GGA GGT TA	This study
Slc16a10	CTG CAG AGG CCA GAT AAG GA	AAG CTA GGG GAC AAG GGA TG	This study
Gypc	CAC GCC TAT CAG CAT ATG GA	GAG ACA GCT ACC ACG GGT GT	This study
Chr 13 140613517	CAG GCT GGG AGA GAA TTT TG	GTA CGC ACT TTG GGG TTT TG	This study
H2AFY3	GGT CCA GGA CAA CGG TTC TA	AGC TCA GGG TGT GAC AGA GG	This study
Ifih1	CCC TTA TCA ATG GCC ACA GT	AAA ACG GAA TCA ACG GTT TG	This study
Dapp1	GCC AAT GCA TAA GTG AGC AA	GGC TTC CGG AAC ACA AGA TA	This study
Accn2	AAT CGG AAA GAT CCC AGC TT	AAT GCA GCC CTC CAT ATC AC	This study
Gfi-1b	GCC CCT GAT AAC ACT TGG AA	GCA ACT GGA GGG AAA TCT GA	This study
Fam125B	TAT GTC TGG TGG CAC ATG CT	GTG ACA GCC AAA GGA GGA AA	This study
Zfpm1	AGC GAT GGG GTT GAT AAG TG	CGG TGA TAA GCA GAG CCT GT	This study
Lyl1	GGG GTC AGC ATT GCT TCT TA	CCT GGC TTC CTC CCT CTT AC	This study
Chr 16 93147915	TAC CCT GGT CTC ACC TCA GC	AGG CAG TGA AGG GGA AAG AT	This study
Pvt1	GAT GTC CCC AGA TAG CCA GA	AGA CTC CAG AAG TGG GCT GA	This study
St3gal	TTG CGA ACA TGC AAA GAT TC	TTT GAG AAG AGT GGG GCA GT	This study
Rap1a	GGT CGT TTG TCT TTC CTC CA	CAG TCT GTC CCC TCC CTA CA	This study
Trem14	GGC CTG CTG AAT TCT CTC TG	GGA GAA GGA ACC TCC TGA CC	This study

1. Lu J, McKinsey TA, Zhang CL, Olson EN (2000) Regulation of skeletal myogenesis by association of the MEF2 transcription factor with class II histone deacetylases. *Mol Cell* 6:233–244.
2. Stopka T, Amanatullah DF, Papetti M, Skoultchi AI (2005) PU.1 inhibits the erythroid program by binding to GATA-1 on DNA and creating a repressive chromatin structure. *EMBO J* 24: 3712–3723.